MICROBIOLOGY

RESEARCH ARTICLE

Subedi *et al.*, *Microbiology* 2022;168:001235

DOI 10.1099/mic.0.001235

MICROBIOLOGY SOCIETY

OPEN ACCESS

Structural characterisation of methanogen pseudomurein cell wall peptide ligases homologous to bacterial MurE/F murein peptide ligases

Bishwa P. Subedi[1,2]†, Linley R. Schofield[1], Vincenzo Carbone[1], Maximilian Wolf[1]‡, William F. Martin[3], Ron S. Ronimus[1,*] and Andrew J. Sutherland-Smith[2,*]

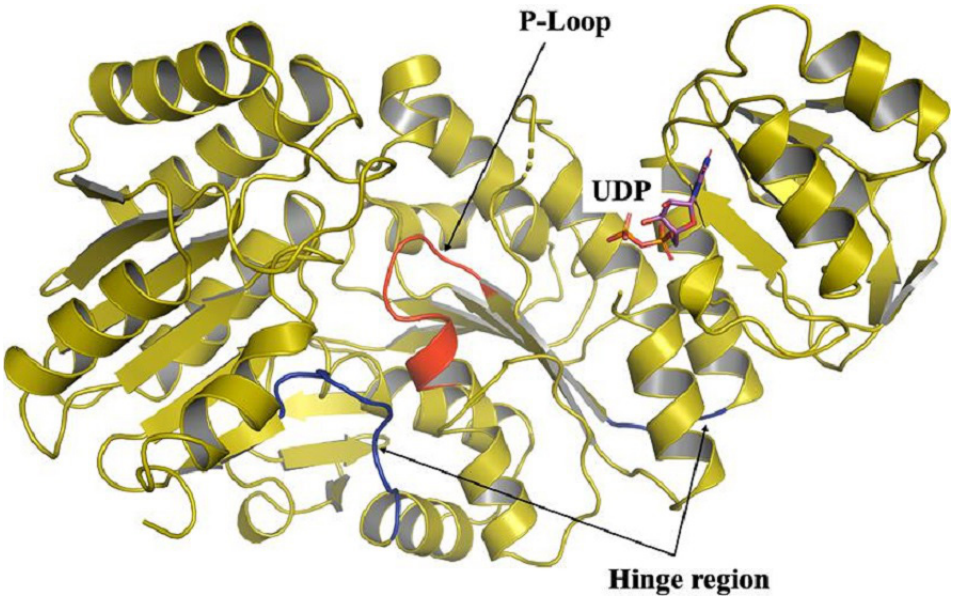

Graphical abstract

Pseudomurein cell wall-containing methanogens have a MurE-like peptide ligase with a homologous structure to bacterial peptidoglycan biosynthesis enzymes. UDP binding, conformational flexibility and active site conservation suggest a shared evolutionary history.

Abstract

Archaea have diverse cell wall types, yet none are identical to bacterial peptidoglycan (murein). Methanogens *Methanobacteria* and *Methanopyrus* possess cell walls of pseudomurein, a structural analogue of murein. Pseudomurein differs from murein in containing the unique archaeal sugar *N*-acetyltalosaminuronic acid instead of *N*-acetylmuramic acid, β–1,3 glycosidic bonds in place of β–1,4 bonds and only L-amino acids in the peptide cross-links. We have determined crystal structures of methanogen pseudomurein peptide ligases (termed pMurE) from *Methanothermus fervidus* (Mfer762) and *Methanothermobacter thermautotrophicus* (Mth734) that are structurally most closely related to bacterial MurE peptide ligases. The homology of the archaeal pMurE and bacterial MurE enzymes is clear both in the overall structure and at the level of each of the three domains. In addition, we identified two UDP-binding sites in Mfer762 pMurE, one at the exterior surface of the interface of the N-terminal and middle domains, and a second site at an inner surface continuous with the highly conserved interface of the three domains. Residues involved in ATP binding in MurE are conserved in pMurE, suggesting that a similar ATP-binding pocket is present at the interface of the middle and the C-terminal domains of pMurE. The presence of pMurE ligases in members of the Methanobacteriales and Methanopyrales, that are structurally related to bacterial MurE ligases, supports the idea that the biosynthetic origins of archaeal pseudomurein and bacterial peptidoglycan cell walls are evolutionarily related.

INTRODUCTION

Cell wall development was a key step in the early evolution of cellular life, with cell walls providing important functions including maintenance of cell shape and protection from osmotic pressure [1]. The differences in cell wall structures and chemistry are some of the major distinguishing features between bacteria and archaea which define them as separate domains in the tree of life [1, 2]. Bacteria have a peptidoglycan (murein) cell wall formed by the polymerization of a glycan-pentapeptide subunit. The enzymatic biosynthesis of peptidoglycan has been well characterized due to its importance as a target for antimicrobial drugs [3, 4]. The peptidoglycan carbohydrate backbone is formed by alternating β–1,4 linked *N*-acetylglucosamine (GlcNAc) and *N*-acetylmuramic acid (MurNAc) residues [2, 5–7]. The addition of the pentapeptide amino acids at the MurNAc is catalysed by four murein peptide ligases (MurC, D, E and F) through a series of ATP-dependent amino acid ligation reactions with a common catalytic mechanism [8, 9]. MurE is responsible for the addition of the third residue to the substrate UDP-*N*-acetyl-α-D-muramoyl-L-alanyl-D-glutamate (UMAG) of the growing peptidoglycan monomer. MurE can vary in substrate specificity typically utilising L-lysine (EC 6.3.2.7) in the majority of Gram-positive bacteria [8], whereas in most Gram-negative bacteria, most cyanobacteria, bacilli and Mycobacteria, MurE (EC 6.3.2.13) adds *meso*-diaminopimelic acid (*m*-DAP) [8, 10–13]. Among the murein peptide ligase types, MurE plays the most crucial role in the pentapeptide formation as the third residue is involved in peptide cross-linking, with the addition of an incorrect amino acid resulting in morphological changes, or even cell lysis [14, 15].

In contrast to the near-omnipresence of murein in bacteria, archaea, dependent on lineage, have a diverse range of cell wall types such as S-layers, methanochondroitin, sulfated-heteropolysaccharides, glutaminylglycan and proteinaceous sheaths [1, 16]. One cell wall type, pseudomurein, has a distribution in archaea limited to the methanogen orders Methanobacteriales and Methanopyrales [1, 17]. Pseudomurein differs from murein in several key respects. First, although its glycan backbone contains *N*-acetylglucosamine (or *N*-acetylgalactosamine in some cases), it utilises a unique archaeal sugar *N*-acetyltalosaminuronic acid [18] instead of MurNAc. In addition, the alternating acetylated monosaccharide residues are β–1,3 linked instead of β–1,4 [19], the pseudomurein cross-linking peptide contains only L-amino acids and has isopeptide bonds [19, 20].

We recently reported gene cluster, taxonomic distribution and phylogenetic analyses of (pseudo)murein peptide ligases indicated to be involved in pseudomurein biosynthesis [21]. Thirteen cell wall biosynthesis enzymes were found to be shared between pseudomurein-containing methanogens and bacteria, with most of the enzymes suggested to have been present in the Last Universal Common Ancestor (LUCA). MurA, MurB, FEM proteins, murein cross-linking transpeptidases and transglycosylases (penicillin-binding proteins (PBPs)), and murein recycling enzymes are not found in pseudomurein-containing methanogens [21]. Another major difference, the gamma-glutamyl-epsilon-lysine cross link in pseudomurein is thought to be catalysed by transglutaminase-like proteins [21, 22]. The peptide ligases (pMurC, pMurD1/D2 and pMurE) were found exclusively in pseudomurein-containing methanogens and the genes are almost always found in two clusters. Cluster one typically contains *pmurD2-pmurD1-pmurC* followed by *vanA/B* and *mobA*-like genes. Cluster two always contains *ddl* (encoding a D-Ala-D-Ala ligase orthologue)-*mraY-pmurE* but can sometimes also contain *pmurC* and/or *pmurD1* as well as two pseudomurein-methanogen-specific conserved genes [21]. This differs largely from (summarised in Subedi *et al*. 2021 [21]) the *E. coli dcw* gene cluster (*mraZ-mraW-ftsL-ftsI-murE-murF-mraY-murD-ftsW-murG-murC-ddl-ftsQ-ftsA-ftsZ* with *murB* being closely associated but separated by more than one intervening gene) and the *Bacillus subtilis* cluster (*mraZ-mraW-ftsL-ftsI-murE-murD-ftsW-murG-murB-ftsQ* with *ftsA-ftsZ* and *murC* being closely associated but separated by more than one intervening gene), with the two methanogen clusters bearing little if any resemblance to the bacterial clusters [21, 23]. For examples, in the pseudomurein-containing methanogens *murG* is never present, the *pmur* peptide ligase genes are almost always split into two clusters, and there are no *fts, mraW* or *mraZ* genes. Structurally, and with respect to the origins of cell wall peptide ligases, the middle and C-terminal domains of pseudomurein peptide ligases are found in the folate biosynthesis enzyme folylpolyglutamate synthase (FPGS) which is widespread amongst bacteria and archaea. FPGS has been suggested to have been a potential precursor to the peptide ligases and is likely to have been

Received 06 May 2022; Accepted 12 July 2022; Published 30 September 2022
Author affiliations: [1]AgResearch Ltd, Grasslands, Tennent Drive, Palmerston North, 4442, New Zealand; [2]School of Natural Sciences, Massey University, Palmerston North 4442, New Zealand; [3]Institute for Molecular Evolution, Heinrich-Heine University Düsseldorf, 40225 Düsseldorf, Germany.
*Correspondence: Ron S. Ronimus, Ron.Ronimus@agresearch.co.nz; Andrew J. Sutherland-Smith, A.J.Sutherland-Smith@massey.ac.nz
Keywords: methanogen; MurE; murein; peptide ligase; pMurE; pseudomurein.
Abbreviations: AS, Australian Synchrotron; BES, N,N-bis(2-hydroxyethyl)-2-aminoethanesulfonic acid; CoM, Coenzyme M; FPGS, Folylpolyglutamate synthase; GlcNac, N-acetylglucosamine; LUCA, Last universal common ancestor; m-DAP, meso-diaminopimelic acid; Mfer, Methanothermus fervidus; MOPS, 3-(N-morpholino)propanesulfonic acid; Mth, Methanothermobactor thermautrophicus; Mur, Murein peptide ligase; MurNAc, N-acetylmuramic acid; NTA, Nitrilotriacetic acid; PBP, Penicillin binding protein; PEG, Polyethylene glycol; pMur, Pseudomurein peptide ligase; rMMS, Randomised microseed matrix screening; RMSD, Root-mean-square deviation; TCEP, Tris(2-carboxyethyl)phosphine; TEA, Triethanolamine; UMAG, UDP-N-acetyl-α-D-muramoyl-L-alanyl-D-glutamate.
†Present address: Faculty of Medicine, Nursing and Health Sciences, Monash Biomedicine Discovery Institute, Monash University, Victoria 3800, Australia
‡Present address: Molecular Enzyme Technology and Biochemistry, Environmental Microbiology and Biotechnology, Centre for Water and Environmental Research, University of Duisburg-Essen, 45141 Essen, Germany.
Three supplementary figures are available with the online version of this article.

Impact Statement

One of the major differences between the bacteria and archaea groups of microorganisms is the structures of their cell walls. We show that methane-producing archaea, that have pseudomurein cells walls of a similar overall architecture using a peptide crosslinked glycan backbone to bacterial peptidoglycan cell walls, have enzymes responsible for pseudomurein synthesis that are similar to those found in bacteria, which suggests a shared evolutionary history.

in LUCA [8, 21]. Overall, the phylogenetic data showed the bacterial and pseudomurein-containing methanogen ligases formed tight well-supported clades with no evidence for recent lateral gene transfer and that cell walls developed early.

Based on gene clustering and phylogenetic data, it is proposed that annotated MurE homologues (pMurE) in pseudomurein-containing methanogens are involved in the ATP-dependent addition of amino acid(s) to the cross-linking pentapeptide chain in the pseudomurein biosynthesis pathway, forming a UDP-N^{α}-glutamyl-γ-phosphate amino acid derivative [20]. The maximum sequence identity between any bacterial MurE and pMurE is 28%, with phylogenetic analysis showing each group clading separately and not able to establish a clear relationship between the bacterial Mur and methanogen pMur enzymes [21]. To clarify the relationship between the bacterial MurE and archaeal pMurE peptide ligases, structures of pMurE have been determined from two different methanogenic archaea, *Methanothermus fervidus* (Mfer762) with and without a substrate analogue (UDP) bound, and *Methanothermobacter thermautotrophicus* ΔH (Mth734). We show that the pMurE structures share clear tertiary structural homology with bacterial MurEs, that a similar ATP-binding pocket is present and suggest that a similar peptide ligase mechanism is used as that described for MurE [8, 24, 25]. Taken together, the structural similarities of the archaeal pMurEs and MurE/F murein peptide ligases reinforce the idea that the pseudomurein biosynthesis pathway shares a deep evolutionary history with that for murein.

METHODS

Protein expression and purification

The *Methanothermus fervidus* (DSM 1088) *Mfer762* sequence (WP_013413839.1) was codon-optimized in the vector pET15b for expression in *E. coli* (Genscript, USA). The *Methanothermobacter thermautotrophicus* ΔH *Mth734* sequence (B69198) was cloned into the pET100D expression vector [26]. Enzyme expression and purification were performed essentially as described by Subedi *et al.* [21] using nickel nitrilotriacetic acid (NTA) chromatography (Jena Bioscience, Germany) of the histidine-tagged recombinant proteins. The final buffer for performing crystallization experiments contained 20 mM MOPS (3-(*N*-morpholino) propanesulfonic acid), pH 7.0, 200 mM KCl and 2 mM TCEP (tris(2-carboxyethyl)phosphine) for both the proteins.

Crystallization and soaking experiments

Crystallization experiments were performed using freshly prepared Mfer762 and Mth734 proteins using the sitting drop method. In total, 75 µl of crystal screening condition was pipetted into plate reservoirs and a drop formed from 1 µl of purified protein and 1 µl of reservoir solution. The crystal condition 0.2 M ammonium sulphate and 30% w/v PEG 4000 at pH 5.4 (SG1 ShotGun screen; Molecular Dimensions, UK) produced hexagonal Mfer762 crystals after 2 weeks (incubated at 21 °C). This crystal condition reproduced similar morphology crystals, and also produced monoclinic crystals in the same drop over a longer period of up to 3 months. Soaking experiments were performed on both Mfer762 crystal forms with 20 mM UDP (prepared in mother liquor) for 10 min. ATP crystal soaking was attempted at a concentration of 25 mM in the presence and absence of 2 mM $MgCl_2$ with no success.

Crystals for Mth734 were obtained by using randomised microseed matrix screening (rMMS). Multiple clusters of needle-shaped crystals obtained from the Morpheus II H7 condition (BES/TEA pH 7.5, 10% w/v PEG 8000, 20% v/v 1,5-pentanediol and polyamines) were used as seeds for rMMS experiments. Mth734 was rescreened in the presence of the seed stock (v/v ratio, 3 protein: 2 reservoir: 1 microseeds) with the Morpheus II screen (Molecular Dimensions, UK). Larger single crystals were obtained in the Morpheus II G10 condition (100 mM amino acids mix; 0.1 M buffer system 6, pH 8.5; 50% v/v precipitant mix of 25% w/v PEG 4000 and 40% w/v 1,2,6-hexanetriol) after 6 months. Both the Mfer762 and Mth734 crystals were harvested in mother liquor with 25% v/v glycerol as cryo-protectant.

Structure determination

X-ray diffraction data for Mfer762-apo and Mfer762-UDP_1 were collected at the Australian Synchrotron (AS) [27] MX1 beamline [28] using an ADSC Quantum 210 r detector. X-ray diffraction data for Mth734 and Mfer762-UDP_2 were collected on the AS MX2 beamline [29] with an EIGER detector [30]. The diffraction data were indexed and integrated using *XDS* [31] followed by data scaling and averaging using *POINTLESS*/*AIMLESS*/*CTRUNCATE* [32, 33] generating a unique data set with a FreeR subset of

Table 1. Data collection and refinement statistics. The values in parentheses represent the values for the highest resolution range.

	Mfer762-APO	Mfer762-UDP_1	Mfer762-UDP_2	Mth734
Resolution range (Å)	34.6–1.8 (1.9–1.8)	34.5–1.9 (2.0–1.9)	41.34–2.0 (2.1–2.0)	47.2–2.9 (3.1–2.9)
Space group	$P6_1$	$P6_1$	$C2$	$P2_1\,2_1\,2_1$
Unit cell (Å / °)	119.8 119.8 70.8 90 90 120	119.4 119.4 71.0 90 90 120	126.8 45.0 98.1 90 98 90	66.0 127.2 134.7 90 90 90
Total reflections	1522905 (141585)	1234378 (115095)	248692 (18725)	342463 (49758)
Unique reflections	50221 (4451)	54413 (5429)	37078 (3578)	25647 (3964)
Multiplicity	22.7 (21.3)	22.7 (21.2)	6.7 (5.2)	13.4 (12.6)
Completeness (%)	99.9 (99.0)	99.9 (99.8)	99.6 (96.7)	99.5 (97.0)
Mean I/sigma (I)	31.9 (1.99)	35.9 (2.2)	15.9 (1.7)	18.8 (3.7)
Wilson B-factor (Å^2)	20.7	22.9	29.0	87.5
R-pim	0.04 (0.43)	0.05 (0.40)	0.06 (0.34)	0.04 (0.30)
$CC_{1/2}$	0.99 (0.59)	0.99 (0.67)	0.99 (0.26)	0.99 (0.83)
CC^*	0.99 (0.86)	0.99 (0.90)	0.99 (0.65)	0.99 (0.83)
Reflections used in refinement	48335 (4451)	45495 (4500)	37040 (3569)	25593 (2568)
Reflections used for R-free	2556 (248)	2381 (210))	1833 (160)	1257 (119)
R_{work}	0.18 (0.27)	0.19 (0.35)	0.18 (0.23)	0.20 (0.31)
R_{free}	0.21 (0.32)	0.23 (0.40)	0.23 (0.26)	0.25 (0.39)
CC_{work}	0.91 (0.86)	0.96 (0.77)	0.96 (0.88)	0.93 (0.70)
CC_{free}	0.96 (0.79)	0.94 (0.72)	0.93 (0.75)	0.91 (0.60)
Number of non-hydrogen atoms	4276	4287	3923	6856
Macromolecules	3863	3831	3689	6825
Ligands	21	54	50	NA
Solvent	392	402	184	31
Protein residues	482	482	469	900
RMS (bonds)	0.007	0.006	0.004	0.009
RMS (angles)	0.86	1.11	0.61	1.59
Ramachandran favoured (%)	96.7	96.7	96.8	94.9
Ramachandran allowed (%)	3.33	3.12	3.2	4.48
Ramachandran outliers (%)	0	0.21	0	0.11
Rotamer outliers (%)	0	0.23	1.22	5.94
Average B-factor (Å^2)	25.0	26.1	34.7	74.9
Protein (Å^2)	24.0	25.1	34.4	73.8
Ligands (Å^2)	39.4	34.8	46.0	NA
Solvent (Å^2)	34.0	34.2	35.6	55.0

5%. The apo and UDP_1 Mfer762 crystals exhibited $P6_1$ symmetry with a single molecule in the asymmetric unit corresponding to 55% solvent. The Mfer762-UDP_2 crystal exhibited $C2$ symmetry with a single molecule in the asymmetric unit corresponding to 53% solvent. A partial model for Mfer762 was initially obtained using domain-based molecular replacement in *MrBUMP* [34] with *Acinetobacter baumannii* MurF (4QDI) as the model placing the Mfer762 middle domain in the asymmetric unit. This partial model was autobuilt with *SHELXE* [35] and *Buccaneer* [36] within *CCP*4i [37], resulting in a nearly complete model for

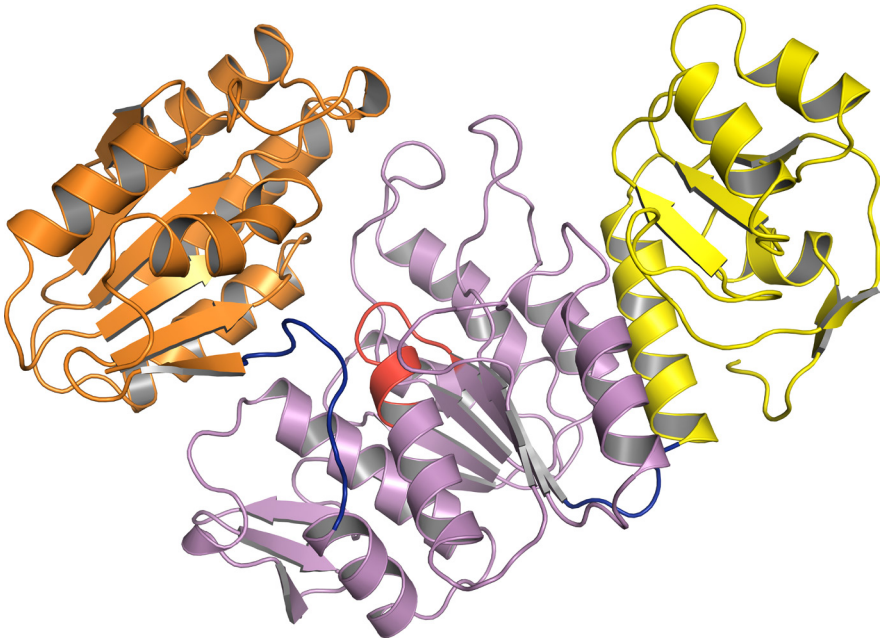

Fig. 1. Cartoon representation of the Mfer762 structure. The N-terminal domain is represented in yellow, the middle domain in purple and the C-terminal domain in orange. Each domain is linked by a hinge region that is represented in blue. The conserved P-loop is shown in red.

Mfer762. Manual rebuilding was performed using *Coot* [38] and refinement was conducted in *REFMAC*5[39] and *PHENIX* [40]. *MOLPROBITY* [41] was used for model validation and the regions indicated as requiring further examination were inspected closely to improve the structure quality. The refined structure of Mfer762-apo was used as a template for molecular replacement using *Phaser* [42] to solve the two UDP-bound Mfer762 structures (Table 1).

X-ray diffraction data collection for Mth734 was processed in the same way as Mfer762 and exhibited $P2_12_12_1$ symmetry consistent with two molecules in the asymmetric unit corresponding to 57% solvent. The structure was solved by molecular replacement in *Phaser* using the Mfer762-apo structure and rebuilt and refined using as for Mfer762. X-ray data and model quality statistics are shown in Table 1. Structure figures have been prepared using PyMOL [43]. Mfer762 and Mth734 atomic coordinates have been deposited in the Protein Data Bank with accession codes Mfer762-apo; 7JT8, Mfer762-UDP_1; 6VR8, Mfer762-UDP_2; 7UFP and Mth734; 7TZI.

Structural similarity and sequence conservation surface analysis

Dali [44] was used to identify structural homologues of Mfer762 and Mth734. Searches were done using the whole tertiary structures and also individual domains of both proteins. The ConSurf server [45] was used to analyse the conservation of related sequences mapped to the Mfer762 structure. The ADP from *M. tuberculosis* MurE (2XJA) was modelled onto Mfer762 based on superposition and structure homology.

RESULTS

Structure of Mfer762

The structure of apo Mfer762 and Mfer762 in complex with UDP are presented in this study. The Mfer762-UDP complex has been solved from two different crystal forms and contains UDP in different binding sites (Mfer762-UDP_1 and Mfer762-UDP_2). The structures of Mfer762-apo and Mfer762-UDP_1 (both $P6_1$ space group) and Mfer762-UDP_2 (*C*2 space group) all contain one molecule in the asymmetric unit (Table 1), with no contact interfaces indicating any oligomeric structure.

The structure of Mfer762 (476 amino acids) comprises three domains (Fig. 1). The Mfer762 N-terminal domain (residues 1–102) folds into a five-stranded mixed β-sheet (β1 anti-parallel, β2-β5 parallel) and four α-helices (α1-α4). The middle domain contains 214 amino acid residues (residues 103–322), which form two β-sheets and eight α-helices (α5-α12). The six stranded (β6-β8 and β11-β13) parallel β-sheet forms the core of the domain, with an adjacent three stranded anti-parallel β-sheet (β14-β16) and a short β-hairpin loop formed by β9 and β10 (G176, W177 and R180, L181, respectively). The middle domain contains a canonical ATP-binding P-loop with conserved sequence $_{110}TGTNGKSTT_{118}$ located between the C-terminus of β6 and the N-terminus of α5

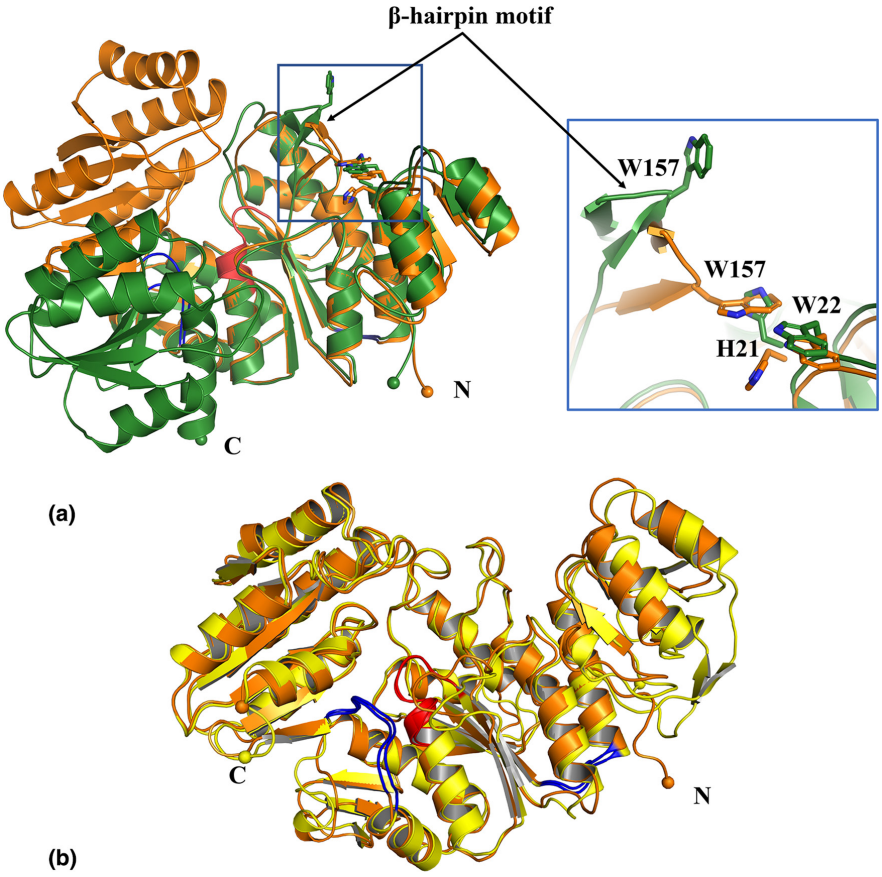

Fig. 2. Structure of Mth734. (a) Superposition of the two Mth734 molecules within the asymmetric unit. Mth734_A is orange, Mth734_B is green, P-loop is red. The C-terminal rigid-body movement is associated with the conformational switch of the middle domain β-hairpin motif containing W157 impacting H21 from the N-terminal domain (stick representation within the zoomed view). (b) Superposition of Mfer762 and Mth734_A (yellow and orange, respectively). The hinge regions between each domain are shown in blue and the P-loop is shown in red for both structures.

at the interface of the middle and the C-terminal domains. Finally, the C-terminal domain consists of 150 amino acids (residues 323–476) forming a Rossmann-like fold that contains one mixed β-sheet (six β-strands; β17-β22) and five α-helices (α13-α17). The Mfer762 structures contain a disulfide bond between C330 and C475 (the penultimate amino acid) in the C-terminal domain. The position of the disulfide bond connects the Mfer762 C-terminus to the N-terminal β17-strand of the C-terminal domain. The conserved P333, located near C330 in the β17-β18 loop, is a *cis*-proline.

Structure of Mth734

The structure of Mth734 was determined in a $P2_12_12_1$ symmetry unit cell containing two monomeric molecules in the asymmetric unit (Table 1). Mth734 shares a homologous tertiary structure and domain topology with Mfer762, also similar to pMurC [21] and the bacterial murein (Mur) ligases. Structural comparison of the two Mth734 molecules in the asymmetric unit reveals a 92° rigid-body rotation of the C-terminal domain of monomer B (Mth734_B) relative to the middle and N-terminal domains, compared to monomer A (Mth734_A). The rotation is centred on the hinge region between the middle and C-terminal domains (Fig. 2a), with the C-terminal domain structures of both monomers equivalent (RMSD 0.35 Å for 148 Cα atoms; for comparison the RMSD of the N-terminal and middle domains combined is 0.70 Å for 292 Cα atoms). The conformational change appears to be associated with crystal packing as steric clashes would result for the C-terminal domain if Mth734_B adopted the same tertiary structure as Mth734_A. The Mth734 middle domain contains a β-hairpin formed by the β8 and β9 strands, a motif that is conserved with Mfer762 (β9-β10). A consequence of the rigid body Mth734_B C-terminal domain rotation is that this β-hairpin motif adopts a different conformation, particularly W157 located on the loop between the two strands. The altered W157 conformation necessitates a change in the rotamer of H21 to avoid a steric clash (Fig. 2a). Rigid-body conformational flexibility for the C-terminal domain is observed for bacterial Mur ligases; *Thermotoga maritima* MurD exhibits different C-terminal domain orientations for the two molecules in the asymmetric unit [46], closure of the C-terminal domain (relative to the rest of the structure) is seen for *Streptococcus pneumoniae*

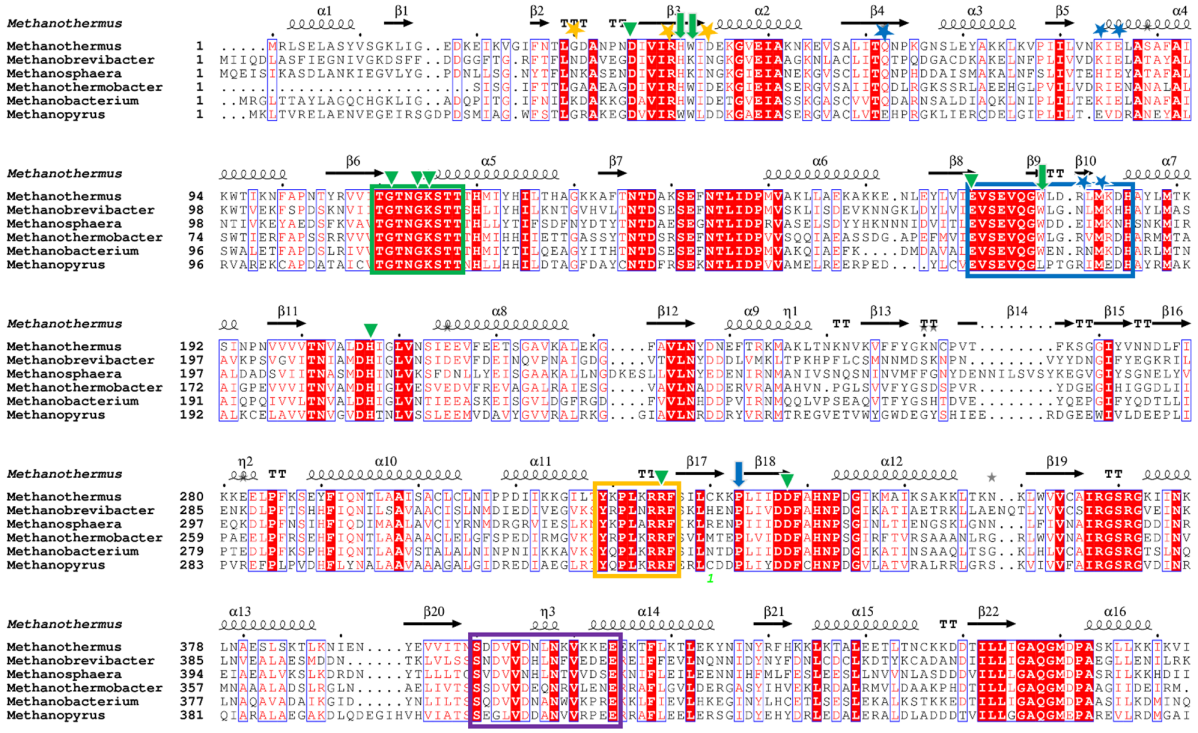

Fig. 3. Structure-based multiple sequence alignment of pMurE peptide ligases. The multiple sequence alignment highlights the key conserved residues of the enzyme class and provides insights to the conserved ATP- and substrate-binding sites. For clarity, sequences of representative species are shown. The pMurE sequences are from *Methanothermus fervidus*, *Methanobrevibacter* sp. AbM4, *Methanosphaera stadtmanae* DSM3091, *Methanothermobacter thermautotrophicus* ΔH, *Methanobacterium* sp. MB1 and *Methanopyrus kandleri* AV19. The pMurE secondary structure is shown in the top row. The conserved P-loop which contributes the residues for ATP binding is represented by a green box. In addition, the residues involved in UDP binding in Mfer762 are highlighted with a star (yellow for UDP_2 and blue for UDP_1 binding sites). The conserved residues forming the 'switch' in pMurE are represented by green down arrows and the hinges by an orange box. The amino acids forming the 'extended loop' of the Mfer762 and the Mth734 structures are also highly conserved and represented by a blue box. The conserved proline observed in *cis*-conformation in both the Mfer762 and Mth734 structures is highlighted by a blue down arrow. The invariable residues that are known to be essential in bacterial murein ligases are also conserved in pMurE and are represented by green triangles. The putative amino acid binding site for pMurE is highlighted by a purple box.

MurF upon inhibitor binding [47] and further analysis is presented by Jung *et al.* [48]. The observation of domain-based rigid-body conformational changes upon inhibitor/substrate binding has led to the proposal of a Mur ligase enzymatic mechanism involving a transition from an open apo structure to a closed substrate-bound conformation [8, 48, 49].

Mth734_A adopts a closed conformation similar to Mfer762 (RMSD 1.2 Å for 442 Cα atoms) and most of the murein ligase structures in the PDB, with the C-terminal domain in a similar orientation (Fig. 2b), while Mth734_B is in a more open structure. Mth734 has a shorter N-terminal domain compared to Mfer762. Mth734 has a homologous P-loop ATP-binding site (Fig. 2b) containing conserved residues (Fig. 3) and similar hinge regions compared to Mfer762. Mth734 also contains a *cis*-proline (P312, Mth734 numbering) in the same position as Mfer762. Structure-based sequence alignment shows the Mfer762 and Mth734 *cis*-proline is strictly conserved as proline for related sequences in all pseudomurein-containing methanogens (Fig. 3).

Analysis of pMur ligase homologues

The C/D and E/F Mur peptide ligase types are distinguished by the different topologies associated with the N-terminal domain [8]. The Mfer762 and Mth734_A N-terminal domains best align with the bacterial MurE/F type peptide ligase structures, with an RMSD of 3.5–5 Å (370–416 Cα atoms) and sequence identities of 18–20% for Mfer762 (Table 2; Fig. 4a–d; Fig S1(available in the online version of this article)) and do not align with MurC/D type N-terminal domain structures. Comparison of the Mfer762 middle domain with the C/D-type pMur Mfer336 [21] shows it to be structurally similar (RMSD 1.6 Å for 216 Cα atoms) with conserved residues forming an ATP-binding site at the interface of the middle and C-terminal domains. The zinc-binding insertion region of the Mfer336 middle domain is not found for Mfer762 (or by sequence alignment in other pMurEs) (Fig. 5a). The Mfer762 C-terminal domain shows structural similarity of RMSD 1.82 Å (138 Cα atoms of 157) to that of Mfer336 (Fig. 5b).

Table 2. Dali [44] structure similarity analysis for the Mfer762-apo tertiary and individual domain structures. The values in each cell represent the Z-score/RMSD (Å) and number of aligned Cα atoms in parentheses; increasing Z-score indicates an increasing degree of confidence in structural similarity. The organism abbreviations are *Haemophilus influenzae* (Hf); *Yersinia pestis* (Yp); *Thermotoga maritima* (Tm); *E. coli* (Ec); *Streptococcus agalactiae* (Sag); *Mycobacterium tuberculosis* (Mt); *Staphylococcus aureus* (Sau); *Pseudomonas aeruginosa* (Pa); *Acinetobacter baumannii* (Ab).

	Mfer762	N-terminal domain	Middle domain	C-terminal domain
Hf-MurC +UMA+ ANP (1P3D)	28.9/3.5 (354)	N/A	20.3/2.3 (178)	14.5/2.5 (131)
Hf-MurC (1GQY)	28.7/3.4 (353)	N/A	19.9/2.3 (172)	14.4/2.5 (131)
Yp-MurC (4HV4)	28.2/3.6 (350)	N/A	20.2/2.3 (171)	14.5/2.6 (133)
Tm-MurC (1J6U)	21.4/4.0 (332)	N/A	17.8/2.7 (168)	13.2/2.2 (115)
Ec-MurC (2F00)	27.8/3.5 (355)	N/A	20.4/2.3 (176)	12.3/2.6 (126)
Ec-MurD (1EEH)	21.5/4.8 (242)	N/A	20.3/2.7 (182)	11.3/2.5 (116)
Ec-MurD (1UAG)	24.1/3.1 (341)	N/A	20.8/2.4 (178)	11.2/2.6 (116)
Ec-MurD (2JFF)	24.4/3.1 (344)	N/A	21.2/2.4 (179)	11.3/2.6 (117)
Sag-MurD (3LK7)	21.8/4.8 (272)	N/A	21.1/2.3 (185)	11.4/2.4 (118)
Tm-MurD (4BUC)	18.7/4.8 (253)	N/A	17.9/2.6 (177)	11.9/2.5 (116)
Mt-MurE (2XJA)	27.6/3.7 (422)	10.3/2.4 (93)	21.2/2.6 (196)	13.5/2.9 (132)
Tm-MurE (4BUB)	26.2/3.4 (395)	9.2/2.4 (87)	19.7/2.7 (188)	15.3/2.2 (129)
Sau-MurE +UML+ ADP (4C12)	26.5/3.2 (407)	8.8/2.6 (87)	22.2/2.4 (196)	13.8/2.8 (130)
Mt-MurE +UAG (2WTZ)	26.7/3.7 (435)	10.2/2.5 (95)	20.8/2.5 (195)	13.5/2.8 (133)
Ec-MurE +UAG+ DAP (1E8C)	28.0/3.6 (427)	6.6/2.9 (81)	20.3/2.6 (194)	15.2/2.4 (132)
Tm-MurF (3ZL8)	30.8/3.0 (427)	4.8/3.0 (69)	21.9/2.0 (191)	11.7/2.7 (117)
Ec-MurF (1GG4)	26.3/5.0 (372)	7.7/2.7 (89)	21.4/2.2 (182)	12.1/2.2 (113)
Pa-MurF (4CVK)	27.9/4.4 (379)	10.3/2.4 (89)	23.5/2.1 (187)	11.9/2.6 (116)
Ab-MurF +ATP (4QF5)	31.7/3.5 (453)	N/A	25.2/1.9 (193)	12.3/2.7 (122)
Ab-MurF +ATP+ UDP (4QDI)	28.3/4.8 (379)	8.1/2.7 (90)	24.4/2.1 (195)	11.9/2.7 (122)

Mfer762 UDP binding (Mfer762-UDP_1)

UDP crystal soaking experiments were performed with the aim of identifying the Mfer762 binding site for the UDP moiety of the UDP-N^{α}-glutamyl-γ-phosphate amino acid derivative substrate. Two Mfer762-UDP structures, in different crystal forms, revealed two distinct UDP-binding sites (Fig. 6a; Fig S2). The structure of Mfer762-UDP_1 is largely equivalent to Mfer762-apo ($P6_1$ space group; RMSD 0.30 Å for 475 Cα atoms) with only a slight shift of the N-terminal domain (Fig. 6a). UDP binding is at a novel Mur/pMur ligase site at the interface of the N-terminal and middle domains formed by the middle domain β-hairpin (β9 and β10, residues 172–184) and the N-terminal domain (β4-α3-β5: Fig. 6b), distinct from sites observed for bacterial Mur structures containing UDP-glycopeptides [11, 50–52]. The carbonyls of the uracil moiety, O2 and O4 form hydrogen bonds with the N-terminal domain's Q62 side-chain Nε and E86 main chain NH, and the Q62 amide oxygen forms a hydrogen bond with the (N3) nitrogen of the uracil ring; these interactions suggest base specificity for uracil. The uracil ring stacks between W177 (middle domain) and the alkyl side-chain region of K84 (Fig. 6b) with the K84 side-chain amine interacting with the UDP β-phosphate. The middle domain M182 side-chain forms a hydrophobic contact with the uracil, and R180 interacts with the ribose O2'. K183 forms sidechain and main chain interactions with the UDP α-phosphate and the L181 main chain oxygen forms a hydrogen bond with the α-phosphate (Fig. S3).

Mfer762 UDP binding (Mfer762-UDP_2)

The Mfer762-UDP_2 structure (space group *C*2) revealed a different UDP-binding site to that of Mfer762-UDP_1, accompanied by structural rearrangements (Fig. 6a). Structural superposition of Mfer762-apo and Mfer762-UDP_2 revealed a rigid-body domain movement of the N-terminal domain relative to the apo and Mfer762-UDP_1 structures (RMSD 1.3 Å, 460 Cα). The Mfer762-UDP_2 UDP-binding site consists of residues solely from the N-terminal domain around β3-α2; T28, L29, G30, R40, I43, D44, K46, G47 and I50 which are within 4.0 Å of the UDP (Fig. 6c). D44 hydrogen bonds to the uracil with its carboxylate group and main chain NH while the R40 side-chain Nε and the G30 main chain NH form electrostatic interactions with the

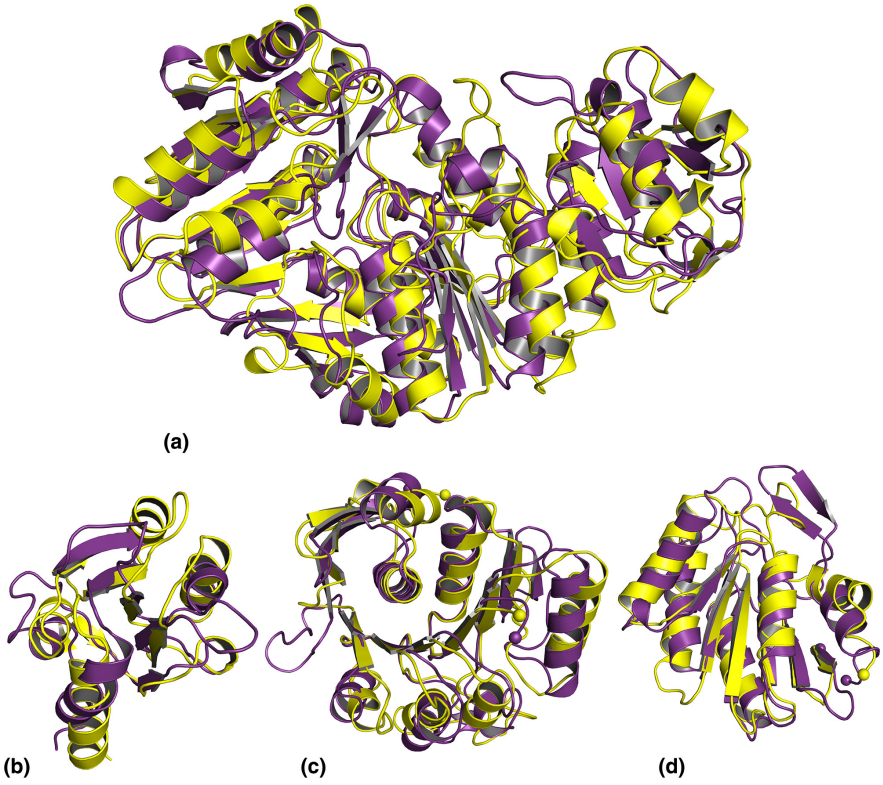

Fig. 4. Structure comparison of Mfer762 with bacterial MurE and MurF; (a) The Mfer762-apo structure (yellow) is superimposed with *E. coli* MurE (1E8C; shown in purple; RMSD 2.76 Å for 382 Cα atoms) and *Acinetobacter baumannii* MurF (4QDI; shown in grey; RMSD 3.40 Å for 352 Cα atoms). Domain comparisons of Mfer762 (yellow) and *E. coli* MurE (1E8C; purple); (b) N-terminal domain, (c) middle domain, (d) C-terminal domain.

UDP phosphates (Fig S3). The Mfer762-UDP_2 N-terminal domain rigid-body movement and rotamer changes of H41 and W42 allow UDP binding at this site and alleviate steric hindrance (Fig. 7). The absence of electron density for the Mfer762-UDP_2 β9-β10 hairpin loop and the different Mth734 structures suggest the interface of the middle and N-terminal domains is a flexible region of pMurE.

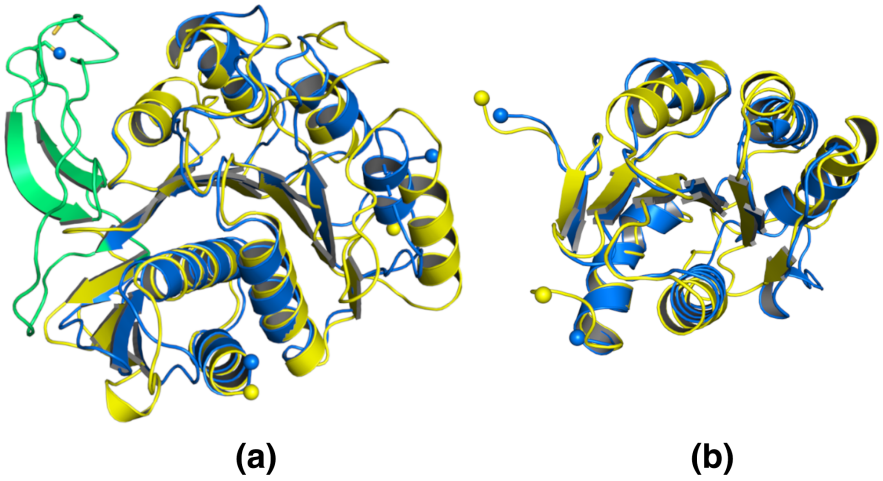

Fig. 5. Comparison of archaeal pMur structures. Superposition of the middle (a) and C-terminal domains (b) of Mfer762 (yellow) and Mfer336 (blue and green). The insertion region of the pMurC Mfer336 structure (6VR7) is shown as green.

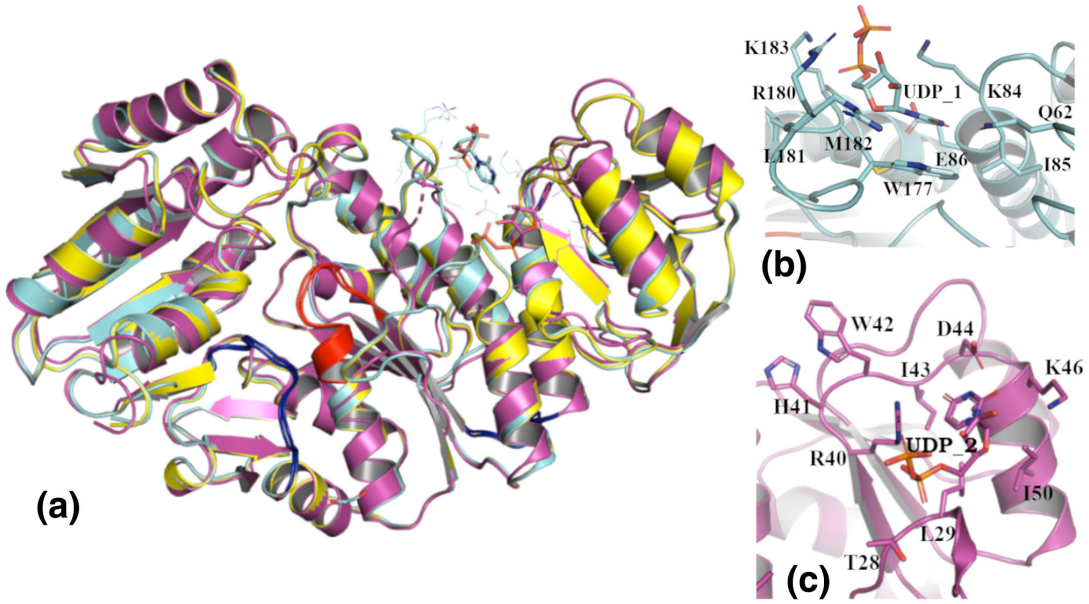

Fig. 6. (a) Structural comparison of Mfer762-apo, Mfer762-UDP_1 and Mfer762-UDP_2. The structure of Mfer762 with UDP bound to the external surface at the interface of the middle and C-terminal domains (Mfer762-UDP_1; cyan) and UDP bound to the internal surface at the N-terminal domain (Mfer762_UDP_2; magenta). The Mfer762-apo structure is yellow. UDP is shown in stick representation with atomic colouring. (b) UDP-binding site of the Mfer762-UDP_1 structure. The residues within 4.0 Å of the UDP are represented as lines and labelled. (c) UDP-binding pocket of the Mfer762-UDP_2 structure. The residues within 4.0 Å are represented as lines and labelled.

DISCUSSION

M. fervidus and *M. thermautotrophicus* ΔH peptide ligase (Mfer762 and Mth734) structures have been determined revealing a three domain tertiary structure homologous to bacterial Mur ligases. Analysis of the Mfer762 and Mth734 N-terminal domains shows that they are structural homologues of the bacterial MurE/F type peptide ligase. Furthermore, Mfer762 and Mth734 (and orthologues) are best described as pMurE peptide ligases, rather than pMurF, based on: 1, Mfer336 has been recently structurally characterised as a methanogen C/D type pMur and has a distinct C/D type N-terminal domain structure [21] in contrast to those of Mfer762 and Mth734. 2, Invariant amino acids present in the Mur ligases [53] are conserved for pMurE including the ATP-binding glycine-rich conserved P-loop (Fig. 3). The presence of these invariant residues in all orthologues of Mfer762 and the structural alignment of these residues for Mfer762 and Mth734 with Mur ligase structures [8, 54] supports Mfer762 and Mth734 being ATP-dependent pseudomurein peptide ligases. 3, Mfer762 and Mth734 share structural similarity with bacterial MurE, whereas the *M. fervidus* and *M. thermautotrophicus* pMur paralogues Mfer1205 and Mth873 have been annotated as pMurF/CfbE. CfbE functions as an amidotransferase, amidating acetate side chains in Ni^{2+}-sirohydrochlorin to generate Ni^{2+}-sirohydrochlorin *a,c*-diamide during the biosynthesis of F_{430} [55, 56], which is required by methyl-CoM reductase in the final step of methane synthesis, hence found in all methanogens including those that do not produce pseudomurein [55]. Additionally, pMurF genes do not cluster with other pseudomurein synthesis genes [57], unlike Mfer762 or Mth734, making it unlikely that methanogen pMurF/CfbE is involved in pseudomurein synthesis.

The conserved domain architecture of the pMurE suggests that the murein and pseudomurein peptide ligases share similar substrate-binding sites and a common ligation mechanism. The inner crescent-shaped surface formed at the interface of the three domains in bacterial murein ligases is used to bind the growing UDP-MurNAc-peptide [8, 58]. A broadly similar surface is present for pseudomurein peptide ligases. The structural opening and closing of Mur ligase structures is facilitated by hinge regions present between each domain [8], with the conformational flexibility, particularly of the C-terminal domain, being evident for pMurE. The Mth734 structure revealed an 'open' and 'closed' structural state of pMurE that might be indicative of a conformational change required for pMur enzyme activity, positioning the ATP, UDP-peptide and amino acid-binding sites in close proximity at the interface of the three domains [50, 58]. Mur peptide ligases catalyse the amino acid ligation through a sequential ordered binding mechanism e.g., for MurE of ATP, UDP-*N*-acetyl-α-D-muramoyl-L-alanyl-D-glutamate (UMAG), then the amino acid (*m*-DAP or L-lysine) [24, 59]. The Mur catalysed reaction proceeds via UDP-glycopeptide carboxyl activation by ATP to form an acyl-phosphate intermediate oriented and stabilised by the ligase and Mg^{2+}. The incoming amino acid is oriented in the active site for ligation via nucleophilic attack forming a tetrahedral intermediate, then the product is released [60]. The enzymatic mechanism is associated with an open apo Mur substrate-binding conformation followed by closure of the

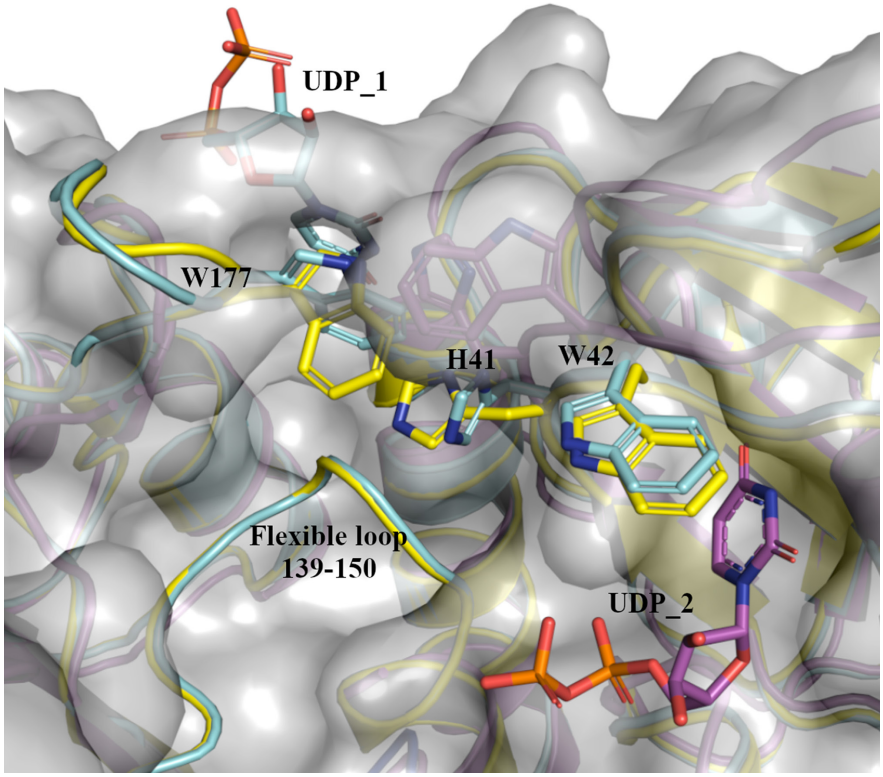

Fig. 7. Surface view (grey) of the UDP_2 binding site of Mfer762-UDP_2 in superposition with the Mfer762-apo (yellow) and Mfer762-UDP_1 (cyan) structures. The conformational change required for UDP_2 (shown in atomic colouring with magenta carbon atoms) binding requires a switch of W42 side-chain rotamer (m-90, yellow and cyan) to p-90 (magenta) to avoid steric hindrance. The Mfer762-apo/UDP_1 conformation of the flexible loop (139-150) would hinder UDP binding at the inner UDP_2 site without rearrangement. W177 and H41 contribute a side-chain switch region connecting the UDP_1 and UDP_2 sites (represented as sticks).

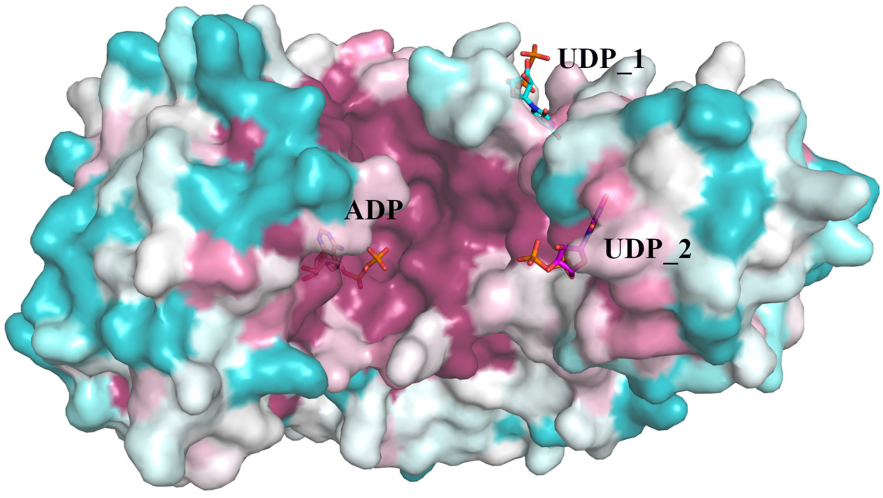

Fig. 8. A ConSurf [45] coloured PyMOL [43] molecular surface representation of the pMurE Mfer762-UDP_2 structure with the UDP_1 and ADP sites additionally superimposed. The protein surface is coloured by ConSurf sequence conservation (purple most conserved, white intermediate and dark cyan the least conserved). The sequence-conserved nature of the continuous surface connecting the UDP_2 and ADP sites is shown.

tertiary structure through the movement of the C-terminal domain towards the middle domain [8]. Rigid-body movement has been observed for the MurD C-terminal domain in the absence of substrates [46, 61] suggesting a relatively low energy barrier for the different conformational states for the Mur [8, 48] and pMurE ligases. The presence of the conserved P-loop ATP-binding site and UDP-binding surface for pMurE suggests that a similar catalytic mechanism is possible for pMurE, but the absence of a successful chemical synthesis of the methanogen pMur N^{α}-UDP-Glu$^{\gamma}$-peptide substrates to date means that the specific pMurE catalytic mechanism remains untested.

The two UDP-bound pMurE structures have implications for understanding the pMurE mechanism. The Mfer762-UDP_1 UDP-binding site is unique amongst all pMur/Mur structures, formed by a β-hairpin region that is conserved for the Mfer762 and Mth734 structures, and as a pMurE sequence insertion in orthologues compared to bacterial MurE sequences. However, the UDP_1 site is not of sufficient size to fit the physiological substrate (N^{α}-UDP-Glu$^{\gamma}$-peptide) and is remote from the ATP-binding site so is unlikely to be the UDP-peptide substrate-binding site. The Mfer762-UDP_2 UDP-binding site is present at the inner surface of the enzyme that interacts solely with the N-terminal domain and requires conformational changes relative to the apo and Mfer762-UDP_1 structures to allow binding. A similar UDP-binding position has been observed for the UDP-glycopeptide substrate for bacterial Mur ligases [11]. The UDP_2 site is more likely to represent the physiological N^{α}-UDP-Glu$^{\gamma}$-peptide substrate-binding site, being of sufficient size, presenting a surface continuous to the ATP-binding/catalytic site to enable generation of the uridine-acyl-phosphate intermediate and being broadly similar to bacterial homologues. ConSurf [45] analysis was performed to map evolutionary conservation of methanogen pMurE sequences onto the Mfer762 structure. The inner surface, including the UDP_2 and ATP-binding sites, is the most conserved region for pMurE further suggesting that this surface is likely to represent the N^{α}-UDP-Glu$^{\gamma}$-peptide binding site (Fig. 8).

Although located on different surfaces of the protein, the two Mfer762 UDP-binding sites are in relatively close proximity, being separated by a side-chain relay of W177, H41 and W42 across the middle and N-terminal domain interface. The middle domain β-hairpin appears to act as a 'switch' region between the middle and N-terminal domains via two structurally conserved residues W177 and H41 (Mfer762). The 'closed switch' conformation adopted by both the Mfer762-apo and Mfer762-UDP_1 structures closes the UDP_2 site. UDP binding at the UDP_1 site results in the stacking of the W177 sidechain with the uracil and movement of the sidechain of H41 which had previously stacked with W177 in the apo state. With H41 in this new p80 rotamer (compared to m-70), W42 cannot undergo the rotamer change as observed in UDP binding at the UDP_2 site (p-90 rotamer), so UDP binding at the UDP_1 site blocks UDP binding at the UDP_2 site (Fig. 7). Whether there is any functional role for the UDP_1 site, for example as a regulatory mechanism, or whether it is a result of adventitious binding is unclear at this stage. The UDP-binding sites are conserved for both Mfer762 and Mth734, and the sequences generally conserved for other pMurE ligases. The Mfer762 H41-W42-W177 side-chain relay is structurally homologous to the Mth734 H21-W22-W157 conformational switch associated with the C-terminal rigid-body movement of one molecule in the asymmetric unit (Fig. 2a). The pMurE structures reveal a side-chain relay located between the middle and N-terminal domains that changes structure upon UDP binding (Mfer762) and C-terminal domain rigid-body movement (Mth734). This relay provides a mechanism that links substrate binding and rigid-body domain conformational changes.

The two different bacterial MurE subtypes EC 6.3.2.13 and EC 6.3.2.7 possess alternate amino acid-binding motifs depending on their substrate specificity, either a DNPR sequence motif for *m*-DAP or a D(D,N)P(N,A) motif for Lys, respectively [11, 25]. pMurE contains neither sequence motif, but instead a sequence insertion at this region suggesting that the amino acid-binding motif for pMurE is distinct to that of MurE. This insertion forms an extended loop between β20 and α14 in the Mfer762 structure which has a conserved sequence of $S_{xxx}V_{xxx}N_xV_{xxx}E$ among pMurE (Fig. 3).

The structure determination of methanogen E type pMur peptide ligases Mfer762 and Mth734 and the previous structure determination of pMurC from *M. fervidus* [21] confirms the presence of both E/F and C/D type archaeal pMur peptide ligases in pseudomurein-containing methanogens providing a direct evolutionary link between bacterial peptidoglycan and archaeal pseudomurein biosynthesis pathways. The pMurE structure analysis shows that key features of the murein peptide ligases are conserved in pseudomurein ligases including ATP and UDP-peptide sites and a tertiary structure that provides a conserved surface and structural flexibility to accommodate the substrates. The discovery of similar pseudomurein pMur peptide ligase architectures suggests a similar enzymatic mechanism to bacterial Mur ligases and that these enzymes share an evolutionary history.

Funding information
This work was supported by the Royal Society of New Zealand Marsden Fund (Grant number AGR1301), the New Zealand Synchrotron Group and the Australian Synchrotron, part of ANSTO, for access to the MX1 and MX2 beamlines. This research was undertaken in part using the MX2 beamline at the Australian Synchrotron, part of ANSTO, and made use of the Australian Cancer Research Foundation (ACRF) detector.

Acknowledgements
We thank the Pastoral Greenhouse gas Research consortium (PGgRc) manager Mark Aspin for support. We thank Professor Dr Bettina Siebers of the University of Duisburg-Essen for help with arranging the BSc research thesis for Maximilian Wolf. We thank Nik Palevich and David Pacheco for critical review of the manuscript.

Author contributions

R.S.R., V.C., L.R.S., B.P.S., W.F.M. and A.J.S.S. contributed to the conception and design of the project. B.P.S., V.C., A.J.S.S., L.R.S., M.W., W.F.M. and R.S.R. contributed to the acquisition, analysis, and interpretation of the data. B.P.S., V.C., A.J.S.S., L.R.S., M.W., W.F.M. and R.S.R. contributed to the writing of the manuscript.

Conflicts of interest

The authors declared that there are no conflicts of interest.

References

1. Albers SV, Meyer BH. The archaeal cell envelope. *Nat Rev Microbiol* 2011;9:414–426.
2. Hartmann E, König H. Comparison of the biosynthesis of the methanobacterial pseudomurein and the eubacterial murein. *Naturwissenschaften* 1990;77:472–475.
3. Bugg TDH, Braddick D, Dowson CG, Roper DI. Bacterial cell wall assembly: still an attractive antibacterial target. *Trends Biotechnol* 2011;29:167–173.
4. Schneider T, Sahl HG. An oldie but a goodie - cell wall biosynthesis as antibiotic target pathway. *Int J Med Microbiol* 2010;300:161–169.
5. König H, Kandler O, Jensen M, Rietschel ET. The primary structure of the glycan moiety of pseudomurein from *Methanobacterium thermoautotrophicum*. *Hoppe Seylers Z Physiol Chem* 1983;364:627–636.
6. König H, Kandler O, Hammes W. Biosynthesis of pseudomurein: isolation of putative precursors from *Methanobacterium thermoautotrophicum*. *Can J Microbiol* 1989;35:176–181.
7. König H, Hartmann E, Kärcher U. Pathways and Principles of the Biosynthesis of Methanobacterial Cell Wall Polymers. *Syst Appl Microbiol* 1993;16:510–517.
8. Smith CA. Structure, function and dynamics in the mur family of bacterial cell wall ligases. *J Mol Biol* 2006;362:640–655.
9. Lovering AL, Safadi SS, Strynadka NCJ. Structural perspective of peptidoglycan biosynthesis and assembly. *Annu Rev Biochem* 2012;81:451–478.
10. Schleifer KH, Kandler O. Peptidoglycan types of bacterial cell walls and their taxonomic implications. *Bacteriol Rev* 1972;36:407–477.
11. Basavannacharya C, Robertson G, Munshi T, Keep NH, Bhakta S. ATP-dependent MurE ligase in Mycobacterium tuberculosis: biochemical and structural characterisation. *Tuberculosis* 2010;90:16–24.
12. Kouidmi I, Levesque RC, Paradis-Bleau C. The biology of Mur ligases as an antibacterial target. *Mol Microbiol* 2014;94:242–253.
13. Patin D, Turk S, Barreteau H, Mainardi J-L, Arthur M, *et al*. Unusual substrate specificity of the peptidoglycan MurE ligase from *Erysipelothrix rhusiopathiae*. *Biochimie* 2016;121:209–218.
14. Mengin-Lecreulx D, Falla T, Blanot D, van Heijenoort J, Adams DJ, *et al*. Expression of the *Staphylococcus aureus* UDP-N-acetylmuramoyl- L-alanyl-D-glutamate:L-lysine ligase in *Escherichia coli* and effects on peptidoglycan biosynthesis and cell growth. *J Bacteriol* 1999;181:5909–5914.
15. Consaul SA, Wright LF, Mahapatra S, Crick DC, Pavelka MS. An unusual mutation results in the replacement of diaminopimelate with lanthionine in the peptidoglycan of a mutant strain of *Mycobacterium smegmatis*. *J Bacteriol* 2005;187:1612–1620.
16. Kandler O, König H. Cell envelopes of archaea: structure and chemistry. In: Kates M, Kushner DJ and Matheson AT (eds). *The Biochemistry of Archaea (Archaebacteria)*. Amsterdam: Elsevier; 1993. pp. 223–259.
17. König H. Archaeobacterial cell envelopes. *Can J Microbiol* 1988;34:395–406.
18. König H, Kandler O. N-Acetyltalosaminuronic acid a constituent of the pseudomurein of the genus *Methanobacterium*. *Arch Microbiol* 1979;123:295–299.
19. Claus H, König H. Cell envelopes of methanogens. In: König H, Claus H and Varma A (eds). *Prokaryotic Cell Wall Compounds: Structure and Biochemistry*. Berlin Springer, 2010. pp. 231–251.
20. Hartmann E, König H. A novel pathway of peptide biosynthesis found in methanogenic Archaea. *Arch Microbiol* 1994;162:430–432.
21. Subedi BP, Martin WF, Carbone V, Duin EC, Cronin B, *et al*. Archaeal pseudomurein and bacterial murein cell wall biosynthesis share a common evolutionary ancestry. *FEMS Microbes* 2021;2:xtab012.
22. Leahy SC, Kelly WJ, Altermann E, Ronimus RS, Yeoman CJ, *et al*. The genome sequence of the rumen methanogen *Methanobrevibacter ruminantium* reveals new possibilities for controlling ruminant methane emissions. *PLoS ONE* 2010;5:e8926.
23. Tamames J, González-Moreno M, Mingorance J, Valencia A, Vicente M. Bringing gene order into bacterial shape. *Trends Genet* 2001;17:124–126.
24. Anderson MS, Eveland SS, Onishi HR, Pompliano DL. Kinetic mechanism of the *Escherichia coli* UDPMurNAc-tripeptide D-alanyl-D-alanine-adding enzyme: use of a glutathione S-transferase fusion. *Biochemistry* 1996;35:16264–16269.
25. Basavannacharya C, Moody PR, Munshi T, Cronin N, Keep NH, *et al*. Essential residues for the enzyme activity of ATP-dependent MurE ligase from *Mycobacterium tuberculosis*. *Protein Cell* 2010;1:1011–1022.
26. Wolf M. *Discovering the pathway of methanogen pseudomurein biosynthesis and the evolutionary correlation to bacterial murein [Bachelor thesis]*. , University of Duisburg-Essen 2011.
27. McPhillips TM, McPhillips SE, Chiu H-J, Cohen AE, Deacon AM, *et al*. Blu-Ice and the distributed control system: software for data acquisition and instrument control at macromolecular crystallography beamlines. *J Synchrotron Radiat* 2002;9:401–406.
28. Cowieson NP, Aragao D, Clift M, Ericsson DJ, Gee C, *et al*. MX1: a bending-magnet crystallography beamline serving both chemical and macromolecular crystallography communities at the Australian Synchrotron. *J Synchrotron Radiat* 2015;22:187–190.
29. Aragão D, Aishima J, Cherukuvada H, Clarken R, Clift M, *et al*. MX2: a high-flux undulator microfocus beamline serving both the chemical and macromolecular crystallography communities at the Australian Synchrotron. *J Synchrotron Radiat* 2018;25:885–891.
30. Casanas A, Warshamanage R, Finke AD, Panepucci E, Olieric V, *et al*. EIGER detector: application in macromolecular crystallography. *Acta Crystallogr D Struct Biol* 2016;72:1036–1048.
31. Kabsch W. XDS. *Acta Crystallogr D Biol Crystallogr* 2010;66:125–132.
32. Evans PR, Murshudov GN. How good are my data and what is the resolution? *Acta Crystallogr D Biol Crystallogr* 2013;69:1204–1214.
33. Evans PR. An introduction to data reduction: space-group determination, scaling and intensity statistics. *Acta Crystallogr D Biol Crystallogr* 2011;67:282–292.
34. Keegan RM, Winn MD. MrBUMP: an automated pipeline for molecular replacement. *Acta Crystallogr D Biol Crystallogr* 2008;64:119–124.
35. Thorn A, Sheldrick GM. Extending molecular-replacement solutions with SHELXE. *Acta Crystallogr D Biol Crystallogr* 2013;69:2251–2256.
36. Cowtan K. The Buccaneer software for automated model building. 1. Tracing protein chains. *Acta Crystallogr D Biol Crystallogr* 2006;62:1002–1011.
37. Winn MD, Ballard CC, Cowtan KD, Dodson EJ, Emsley P, *et al*. Overview of the CCP4 suite and current developments. *Acta Crystallogr D Biol Crystallogr* 2011;67:235–242.
38. Emsley P, Lohkamp B, Scott WG, Cowtan K. Features and development of Coot. *Acta Crystallogr D Biol Crystallogr* 2010;66:486–501.
39. Murshudov GN, Skubák P, Lebedev AA, Pannu NS, Steiner RA, *et al*. REFMAC5 for the refinement of macromolecular crystal structures. *Acta Crystallogr D Biol Crystallogr* 2011;67:355–367.

40. Liebschner D, Afonine PV, Baker ML, Bunkóczi G, Chen VB, *et al*. Macromolecular structure determination using X-rays, neutrons and electrons: recent developments in Phenix. *Acta Crystallogr D Struct Biol* 2019;75:861–877.
41. Davis IW, Murray LW, Richardson JS, Richardson DC. MOLPROBITY: structure validation and all-atom contact analysis for nucleic acids and their complexes. *Nucleic Acids Res* 2004;32:W615-9.
42. McCoy AJ, Grosse-Kunstleve RW, Adams PD, Winn MD, Storoni LC, *et al*. Phaser crystallographic software. *J Appl Crystallogr* 2007;40:658–674.
43. Schrödinger L. *The PyMOL Molecular Graphics System*. Version 1.8. Schrödinger, LLC,
44. Holm L, Laakso LM. Dali server update. *Nucleic Acids Res* 2016;44:W351-5.
45. Landau M, Mayrose I, Rosenberg Y, Glaser F, Martz E, *et al*. ConSurf 2005: the projection of evolutionary conservation scores of residues on protein structures. *Nucleic Acids Res* 2005;33:W299-302.
46. Favini-Stabile S, Contreras-Martel C, Thielens N, Dessen A. MreB and MurG as scaffolds for the cytoplasmic steps of peptidoglycan biosynthesis. *Environ Microbiol* 2013;15:3218–3228.
47. Longenecker KL, Stamper GF, Hajduk PJ, Fry EH, Jakob CG, *et al*. Structure of MurF from *Streptococcus pneumoniae* co-crystallized with a small molecule inhibitor exhibits interdomain closure. *Protein Sci* 2005;14:3039–3047.
48. Jung KH, Kim Y-G, Kim CM, Ha HJ, Lee CS, *et al*. Wide-open conformation of UDP-MurNc-tripeptide ligase revealed by the substrate-free structure of MurE from *Acinetobacter baumannii*. *FEBS Lett* 2021;595:275–283.
49. El Zoeiby A, Sanschagrin F, Levesque RC. Structure and function of the Mur enzymes: development of novel inhibitors. *Mol Microbiol* 2003;47:1–12.
50. Gordon E, Flouret B, Chantalat L, van Heijenoort J, Mengin-Lecreulx D, *et al*. Crystal structure of UDP-N-acetylmuramoyl-L-alanyl-D-glutamate: meso-diaminopimelate ligase from *Escherichia coli*. *J Biol Chem* 2001;276:10999–11006.
51. Ruane KM, Lloyd AJ, Fülöp V, Dowson CG, Barreteau H, *et al*. Specificity determinants for lysine incorporation in *Staphylococcus aureus* peptidoglycan as revealed by the structure of a MurE enzyme ternary complex. *J Biol Chem* 2013;288:33439–33448.
52. Cha SS, An YJ, Jeong CS, Yu JH, Chung KM. ATP-binding mode including a carbamoylated lysine and two Mg(2+) ions, and substrate-binding mode in *Acinetobacter baumannii* MurF. *Biochem Biophys Res Commun* 2014;450:1045–1050.
53. Bouhss A, Mengin-Lecreulx D, Blanot D, van Heijenoort J, Parquet C. Invariant amino acids in the Mur peptide synthetases of bacterial peptidoglycan synthesis and their modification by site-directed mutagenesis in the UDP-MurNAc:L-alanine ligase from *Escherichia coli*. *Biochemistry* 1997;36:11556–11563.
54. Mol CD, Brooun A, Dougan DR, Hilgers MT, Tari LW, *et al*. Crystal structures of active fully assembled substrate- and product-bound complexes of UDP-N-acetylmuramic acid:L-alanine ligase (MurC) from *Haemophilus influenzae*. *J Bacteriol* 2003;185:4152–4162.
55. Zheng K, Ngo PD, Owens VL, Yang XP, Mansoorabadi SO. The biosynthetic pathway of coenzyme F430 in methanogenic and methanotrophic archaea. *Science* 2016;354:339–342.
56. Moore SJ, Sowa ST, Schuchardt C, Deery E, Lawrence AD, *et al*. Elucidation of the biosynthesis of the methane catalyst coenzyme F_{430}. *Nature* 2017;543:78–82.
57. Subedi BP. *Structural and functional studies of pseudomurein peptide ligases in methanogenic archaea: a dissertation presented in partial fulfilment of the requirements for the degree of Doctor of Philosophy in Biochemistry [Doctoral thesis]*. , Massey University, Manawatu, New Zealand; 2018.
58. Deva T, Baker EN, Squire CJ, Smith CA. Structure of *Escherichia coli* UDP-N-acetylmuramoyl:L-alanine ligase (MurC). *Acta Crystallogr D Biol Crystallogr* 2006;62:1466–1474.
59. Emanuele JJ, Jin H, Yanchunas J, Villafranca JJ. Evaluation of the kinetic mechanism of *Escherichia coli* uridine diphosphate-N-acetylmuramate:L-alanine ligase. *Biochemistry* 1997;36:7264–7271.
60. Bertrand JA, Auger G, Martin L, Fanchon E, Blanot D, *et al*. Determination of the MurD mechanism through crystallographic analysis of enzyme complexes. *J Mol Biol* 1999;289:579–590.
61. Šink R, Kotnik M, Zega A, Barreteau H, Gobec S, *et al*. Crystallographic study of peptidoglycan biosynthesis Enzyme MurD: domain movement revisited. *PLoS One* 2016;11:e0152075.

Edited by: W. van Schaik and H. Strahl